

Patterns and ecological drivers of ocean viral communities

Jennifer R. Brum,^{1*}† J. Cesar Ignacio-Espinoza,^{2*}† Simon Roux,^{1*}†
 Guilhem Doucier,^{1,3} Silvia G. Acinas,⁴ Adriana Alberti,⁵ Samuel Chaffron,^{6,7,8}
 Corinne Cruaud,⁵ Colombar de Vargas,^{9,10} Josep M. Gasol,⁴ Gabriel Gorsky,^{11,12}
 Ann C. Gregory,¹³† Lionel Guidi,^{11,12} Pascal Hingamp,¹⁴ Daniele Iudicone,¹⁵
 Fabrice Not,^{9,10} Hiroyuki Ogata,¹⁶ Stéphane Pesant,^{17,18} Bonnie T. Poulos,¹
 Sarah M. Schwenck,¹ Sabrina Speich,¹⁹† Celine Dimier,^{9,10,20} Stefanie Kandels-Lewis,^{21,22}
 Marc Picheral,^{11,12} Sarah Searson,^{11,12} Tara Oceans Coordinators,§ Peer Bork,^{21,23}
 Chris Bowler,²⁰ Shinichi Sunagawa,²¹ Patrick Wincker,^{5,24,25}
 Eric Karsenti,^{20,22}|| Matthew B. Sullivan^{1,2,13,†}||

Viruses influence ecosystems by modulating microbial population size, diversity, metabolic outputs, and gene flow. Here, we use quantitative double-stranded DNA (dsDNA) viral-fraction metagenomes (viromes) and whole viral community morphological data sets from 43 Tara Oceans expedition samples to assess viral community patterns and structure in the upper ocean. Protein cluster cataloging defined pelagic upper-ocean viral community pan and core gene sets and suggested that this sequence space is well-sampled. Analyses of viral protein clusters, populations, and morphology revealed biogeographic patterns whereby viral communities were passively transported on oceanic currents and locally structured by environmental conditions that affect host community structure. Together, these investigations establish a global ocean dsDNA viromic data set with analyses supporting the seed-bank hypothesis to explain how oceanic viral communities maintain high local diversity.

Ocean microbes produce half of the oxygen we breathe (1) and drive much of the substrate and redox transformations that fuel Earth's ecosystems (2). However, they do so in a constantly evolving network of chemical, physical, and biotic constraints—interactions that are only beginning to be explored. Marine viruses are presumably key players in these interactions (3, 4), as they affect microbial populations through lysis, reprogramming of host metabolism, and horizontal gene transfer. Here, we strive to develop an overview of ocean viral community patterns and ecological drivers.

The Tara Oceans expedition provided a platform for sampling ocean biota from viruses to fish larvae within a comprehensive environmental context (5). Prior virus-focused work from this expedition has helped optimize the double-stranded DNA (dsDNA) viromic sample-to-sequence workflow (6), evaluate ecological drivers of viral community structure as inferred from morphology (7), and map ecological patterns in the large dsDNA nucleocytoplasmic viruses using marker genes (8). Here, we explore global patterns and structure of ocean viral communities using 43 samples from 26 stations in the Tara Oceans expedition (see supplementary file S1) to establish dsDNA viromes from viral-fraction (<0.22 μm) concentrates and quantitative whole viral community morphological data sets from unfiltered seawater. Viruses lack shared genes that can be used for investigation of community patterns. Therefore, we used three levels of information to study such patterns: (i) protein clusters (PCs) (9) as a means to organize

virome sequence space commonly dominated by unknown sequences (63 to 93%) (10), (ii) populations, using established metrics for viral contig recruitment (11), and (iii) morphology, using quantitative transmission electron microscopy (qTEM) (7).

The Tara Oceans Viromes (TOV) data set

The 43 Tara Oceans Viromes (TOV) data set comprises 2.16 billion ~101-base pair (bp) paired-end Illumina reads (file S1), which largely represent epipelagic ocean viral communities from the surface (ENVO:00002042) and deep chlorophyll maximum (DCM; ENVO:01000326) throughout seven oceans and seas; only 1 of 43 viromes is from mesopelagic waters, Environment Ontology feature ENVO:0000213 (file S1). The TOV data set offers deeper sampling of surface ocean viral communities but underrepresents the deep ocean relative to the Pacific Ocean Viromes data set (POV) (10), which includes 16 viromes from aphotic zone waters. In all viromes, sampling and processing affects which viruses are represented (6, 12–14). We filtered TOV seawater samples through 0.22-μm-pore-sized filters and then concentrated viruses in the filtrate using iron chloride flocculation (15). These steps would have removed most cells but also would have excluded any viruses larger than 0.22 μm. We then purified the resulting TOV viral concentrates using deoxyribonuclease (DNase) treatment, which is as effective as density gradients for purifying ocean viral concentrates (14). This DNase-only step is unlikely to affect viral representation in the viromes but reduces nonviral DNA contamination. Finally, we extracted DNA from the samples and

prepared sequence libraries using linker amplification (13). These steps preserve quantitative representation of dsDNA viruses in the resulting viromes (12, 13), but the ligation step excludes RNA viruses and is biased against single-stranded DNA (ssDNA) viruses (12).

We additionally applied quantitative transmission electron microscopy (qTEM) (7) to paired whole seawater samples to evaluate patterns in whole viral communities. This method simultaneously considers ssDNA, dsDNA, and RNA viruses, although without knowledge of their relative abundances because particle morphology does not identify nucleic acid type. In the oceans, total virus abundance estimates based on TEM analyses, which include all viral particles, are similar to estimates based on fluorescent staining, which inefficiently stains ssDNA and RNA viruses (16–24). This suggests that most

¹Department of Ecology and Evolutionary Biology, University of Arizona, Tucson, AZ 85721, USA. ²Department of Molecular and Cellular Biology, University of Arizona, Tucson, AZ 85721, USA. ³Environmental and Evolutionary Genomics Section, Institut de Biologie de l'École Normale Supérieure (IBENS), CNRS, UMR8197, INSERM U1024, 75230 Paris, France. ⁴Department of Marine Biology and Oceanography, Institute of Marine Sciences (ICM-CSIC), Pg. Marítim de la Barceloneta 37-49, Barcelona, E08003, Spain. ⁵Genoscope, Commissariat à l'Énergie Atomique (CEA)—Institut de Génétique, 2 rue Gaston Crémieux, 91057 Evry, France. ⁶Department of Microbiology and Immunology, Rega Institute, KU Leuven, Herestraat 49, 3000 Leuven, Belgium. ⁷Center for the Biology of Disease, VIB KU Leuven, Herestraat 49, 3000 Leuven, Belgium. ⁸Department of Applied Biological Sciences, Vrije Universiteit Brussel, Pleinlaan 2, 1050 Brussels, Belgium. ⁹CNRS, UMR 7144, Station Biologique de Roscoff, Place Georges Teissier, 29680 Roscoff, France. ¹⁰Sorbonne Universités, Université Pierre et Marie Curie, Université Paris 06, and UMR 7144, Station Biologique de Roscoff, Place Georges Teissier, 29680 Roscoff, France. ¹¹CNRS, UMR 7093, Laboratoire d'océanographie de Villefranche (LOV), Observatoire Océanologique, 06230 Villefranche-sur-mer, France. ¹²Sorbonne Universités, Université Pierre et Marie Curie, Université Paris 06, UMR 7093, Laboratoire d'océanographie de Villefranche (LOV), Observatoire Océanologique, 06230 Villefranche-sur-mer, France. ¹³Soil, Water, and Environmental Science, University of Arizona, Tucson, AZ 85721, USA. ¹⁴Aix Marseille Université, CNRS IGS UMR 7256, 13288 Marseille, France. ¹⁵Stazione Zoologica Anton Dohrn, Villa Comunale, 80121 Naples, Italy. ¹⁶Institute for Chemical Research, Kyoto University, Gokasho, Uji, Kyoto 611-0001, Japan. ¹⁷PANGAEA, Data Publisher for Earth and Environmental Science, University of Bremen, 28359 Bremen, Germany. ¹⁸MARUM, Center for Marine Environmental Sciences, University of Bremen, 28359 Bremen, Germany. ¹⁹Laboratoire de Physique des Océans, Institut Universitaire Européen de la Mer, Université de Bretagne Occidentale (UBO-IUEM), Place Copernic, 29820 Plouzané, France. ²⁰Institut de Biologie de l'École Normale Supérieure (IBENS), and INSERM U1024, and CNRS UMR 8197, Paris, 75005, France. ²¹Structural and Computational Biology, European Molecular Biology Laboratory, Meyerhofstrasse 1, 69117 Heidelberg, Germany. ²²Directors' Research, European Molecular Biology Laboratory Meyerhofstrasse 1, 69117 Heidelberg, Germany. ²³Max-Delbrück-Centre for Molecular Medicine, 13092 Berlin, Germany. ²⁴CNRS, UMR 8030, CP5706, 91057 Evry, France. ²⁵Université d'Evry, UMR 8030, CP5706, 91057 Evry, France. *These authors contributed equally to this work. †Present address: Department of Microbiology, Ohio State University, Columbus, OH 43210, USA. ‡Present address: Department of Geosciences, Laboratoire de Météorologie Dynamique (LMD), École Normale Supérieure, 24 rue Lhomond 75231 Paris, Cedex 05, France. §Tara Oceans coordinators and affiliations are listed after the Acknowledgments. ||Corresponding authors. E-mail: mbsulli@gmail.com (M.B.S.); karsenti@embl.de (E.K.)

ocean viruses are dsDNA viruses. However, one study quantifying nucleic acids at a single marine location suggests that RNA viruses may constitute as much as half of the viral community there (16). It remains unknown what the relative contribution of these viral types is to the whole viral community, but our analyses suggest small dsDNA viruses likely dominate as follows. The viromes capture the <0.22- μm dsDNA viruses of bacteria and archaea that are thought to dominate marine viral communities, whereas qTEM analysis includes all viruses regardless of size, nucleic acid type, or host (7). In these whole seawater samples used for qTEM, we found that viral capsid diameters ranged from 26 to 129 nm, with the per-sample average capsid diameter constrained at 46 to 66 nm (Fig. 1). We detected no viral particles larger than 0.22 μm among 100 randomly counted particles from each of 41 qTEM samples. These findings are similar to those from a subset of these Tara Oceans stations (14 of the 26 stations) (7) and indicate that size fractionation using 0.22- μm filtration to prepare viromes did not substantially bias the TOV data set.

TOV protein clusters for comparison of local and global genetic richness and diversity

Across the 43 viromes, a total of 1,075,763 PCs were observed, with samples beyond the 20th virome adding few PCs (Fig. 2A). When we combined TOV with 16 photic-zone viromes from the POV data set (10), the number of PCs increased to 1,323,921 but again approached a plateau (Fig. 2B). These results suggest that, although it is impossible to sample completely, the sequence space corresponding to dsDNA viruses from the epipelagic ocean is now relatively well sampled. This contrasts results from marine microbial metagenomic surveys using older sequencing technologies (9) but is consistent with those from this expedition (25), as well as findings from viral sequence data sets that suggest a limited range of functional diversity derived from bacterial and archaeal viral isolates (26) and the POV data set (27).

PCs were next used to establish the core genes shared across the TOV data set (Fig. 2A). Broadly, there were 220, 710, and 424 core PCs shared across all surface and DCM viromes, surface viromes only, and DCM viromes only, respectively. The number of core PCs in the upper-ocean TOV samples (220 PCs) was thus less than the number of photic-zone core PCs in POV (565 PCs) (28), likely because the POV data set includes only the Pacific Ocean, whereas TOV includes samples from seven oceans and seas. However, the number of core PCs in the upper-ocean TOV samples exceeded the total number of core PCs observed in POV (180 PCs) (28), likely because of deep-ocean representation in POV (half of the samples in POV are from the aphotic zone). Consistent with the latter finding, the addition of the sole deep-ocean TOV sample, TARA_70_MESO, decreased the number of core PCs shared by all TOV samples from 220 to 65, which suggests that deep-

ocean viral genetic repertoires are different from those in the upper oceans. Indeed, niche-differentiation has been observed in viromes sampled across these oceanic zones in the POV data set (28), and similar findings were observed in the microbial metagenomic counterparts from the Tara Oceans Expedition (25). Thus, viral communities from the deep ocean remain poorly explored and appear to hold different gene sets from those in the epipelagic oceans.

Beyond core and pan metagenomic analyses, PCs also provide a metric for viral community diversity comparisons (Fig. 3A and file S1) from which three trends emerge in the TOV data set. First, high-latitude viromes (82_DCM and 85_DCM) were least diverse [the entropy calculated with the natural log of diversity, Shannon's H' , of 8.93 and 9.22 natural digits (nats)], consistent with patterns in marine macroorganisms (29) and epipelagic ocean bacteria (25, 30). Second, the remaining viromes had similar diversity (Shannon's H' between 9.47 and 10.55 nats) and evenness (Pielou's J from 0.85 to 0.91), which indicated low dominance of any particular PCs (31). Third, local diversity was relatively similar to global diversity (local:global ratios of H' from 0.73 to 0.87), which suggested high dispersal of viral genes (32) across the sampled ocean viral communities.

TOV viral populations for assessing global viral community structure

We next estimated abundances of the 5476 dominant viral populations in TOV, which represented up to 9.97% of aligned reads in a sample

and were defined by applying empirically derived recruitment cut-offs from naturally occurring T4-like cyanophages (11) to high-confidence contigs from bacterial and archaeal viruses (see Methods). Assigning viral populations on the basis of virome data remains challenging (11, 33), but here, the assembly of large contigs (up to 100 kb) aided our ability to accomplish not only analyses at the gene-level using PCs but also the genome-level using viral populations. Viral populations were rarely endemic to one station (15%) and, instead, were commonly observed across >4 stations (47%) and up to 24 of the 26 stations (Figs. 4 and 5A). Exceptional samples include those from the Benguela upwelling region (TARA_67_SUR) and high-latitude samples from the Falklands and Antarctic Circumpolar currents (TARA_82_DCM and TARA_85_DCM, respectively). These samples were also divergent when we assessed microbial communities (TARA_82_DCM and TARA_85_DCM displayed lower microbial genetic richness) (25) and eukaryotic communities (TARA_67_SUR had specific and unique eukaryotic communities in all size fractions) (34). Although many viral populations were broadly distributed, they were much more abundant at the original location (origin inferred from longest contig assembled; see Methods) compared with alternate stations (Fig. 5B). Thus, most populations were relatively widespread but with variable sample-to-sample abundances. As was observed with PCs, diversity and evenness estimates based on viral populations were similar across all samples except for high-latitude samples (TARA_82_DCM and

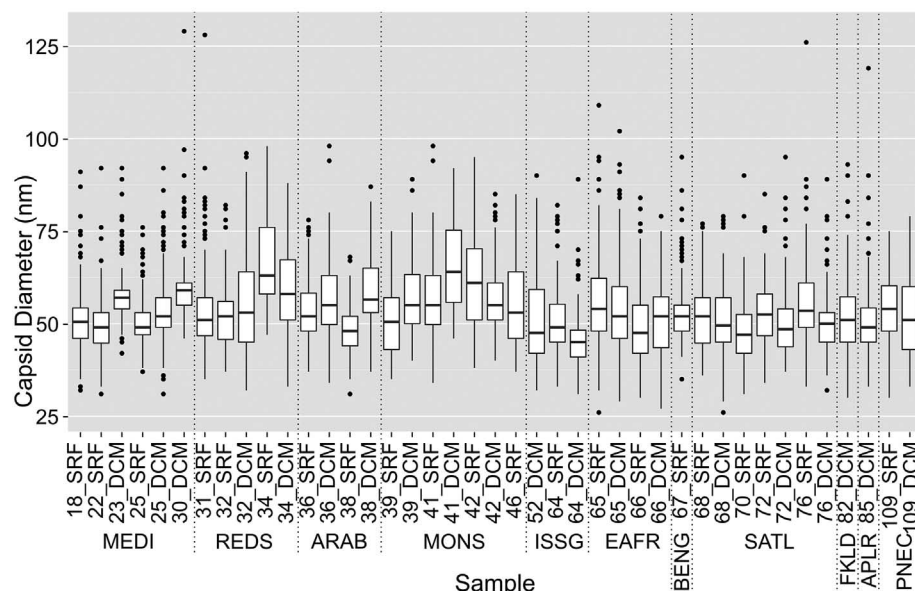


Fig. 1. Distribution of viral capsid diameters in each sample ($n = 100$ viruses per sample). Data are not available for samples TARA_18_DCM and TARA_70_MESO. Boxplots are constructed with the upper and lower lines corresponding to the 25th and 75th percentiles; outliers are displayed as points. Longhurst provinces are indicated below samples (MEDI, Mediterranean Sea; REDS, Red Sea; ARAB, NW Arabian Upwelling; MONS, Indian Monsoon Gyres; ISSG, Indian S. Subtropical Gyre; EAFR, E. Africa Coastal; BENG, Benguela Current Coastal; SATL, S. Atlantic Gyre; FKLD, SW Atlantic Shelves; APLR, Austral Polar; PNEC, N. Pacific Equatorial Countercurrent).

TARA_85_DCM) and one sample in the Red Sea (TARA_32_DCM) that displayed lower diversity (Fig. 3B and file S1). Finally, local diversity was relatively similar to global diversity (local:global ratios of H' from 0.23 to 0.86, average 0.74) (file S1) and reflected the high dispersal of viruses as highlighted by PC analysis.

Only 39 of the 5476 populations we identified could be affiliated to cultured viruses, which reflects the dearth of reference viral genomes in databases. These cultured viruses include those infecting the abundant and widespread hosts SARI1, SARI16, *Roseobacter*, *Prochlorococcus*, and *Synechococcus* (Fig. 6). The most abundant and widespread viral populations observed in TOV lack cultured representatives (Fig. 6), which suggests that most upper-ocean viruses remain to be characterized even though viruses from known dominant microbial hosts (35–39) have been cultured. Methods independent of cultivation—

including viral tagging (11) and mining of microbial genomic data sets (40, 41)—show promise to expand the number of available viral reference genomes (33).

Drivers of global viral community composition and distribution

We next leveraged this global data set to evaluate ecological drivers (including environmental variables, sample location, and microbial abundances) (file S1) of viral community structure using all three data types—morphology, populations, and PCs. These metrics revealed increasing resolution, respectively, and showed that viral community structure was influenced by region and/or environmental conditions (Table 1). We conducted the analysis of ecological drivers using all samples in this study, as well as a sample subset that omitted samples with exceptional environmental conditions and divergent viral commu-

nities observed using PC and population analyses (see above; TARA_67_SUR, TARA_82_DCM, TARA_85_DCM, and TARA_70_MESO). Within the sample subset, oceanic viral communities varied significantly with Longhurst province, biome, latitude, temperature, oxygen concentration, and microbial concentrations (including total bacteria, *Synechococcus*, and *Prochlorococcus*). Viral communities were not structured by depth (surface versus DCM) except when considering PCs, which likely reflects the minimal variation between samples in the epipelagic zone compared with that of globally sourced samples, as well as the higher resolution provided by PCs. Nutrients influenced viral community structure when we considered the whole data set but were much less explanatory when the few high-nutrient samples were removed, except for the influence of phosphate concentration on viral populations. Thus, nutrient concentrations may influence viral community structure, but testing this hypothesis would require analysis of samples across a more continuous nutrient gradient.

Global-scale analyses of oceanic macro- (29) and microorganisms (30) have been conducted, including a concurrent *Tara* Oceans study showing that temperature and oxygen influence microbial community structure (25). Environmental conditions have also been shown to affect global viral community morphological traits (7). Our TOV study is consistent with these earlier findings in that viral communities are influenced by temperature and oxygen concentration, but not chlorophyll concentration (Table 1). Biogeographic structuring of TOV viral communities on the basis of the significant influence of latitude and Longhurst provinces is also consistent with the conclusion that geographic region influences community structure in Pacific Ocean viruses (42). Although only PC analysis showed depth-based divergence, this likely reflects poor ($n = 1$) deep sample representation in the TOV data set as discussed above. Prior POV viral investigation and concurrent *Tara* Oceans microbial analysis, both of which have better deep-water representation, show stronger depth patterns whereby photic and aphotic zone communities diverge (25, 28, 42). Thus, our results suggest that the biogeography of upper-ocean viral communities is structured by environmental conditions.

Because viruses require host organisms to replicate, viral community structure follows from environmental conditions shaping the host community, as observed in paired *Tara* Oceans microbial samples (25), which would then indirectly affect viral community composition. However, global distribution of viruses can also be directly influenced by environmental conditions, such as salinity, that affect their ability to infect their hosts (43). Additionally, the variable decay rates observed for cultivated viruses and whole viral communities (44) could also influence their distribution as viruses with lower inherent decay rates will persist for longer in the environment, and environments with more favorable conditions (such as fewer extracellular enzymes) will also contribute to increased viral persistence.

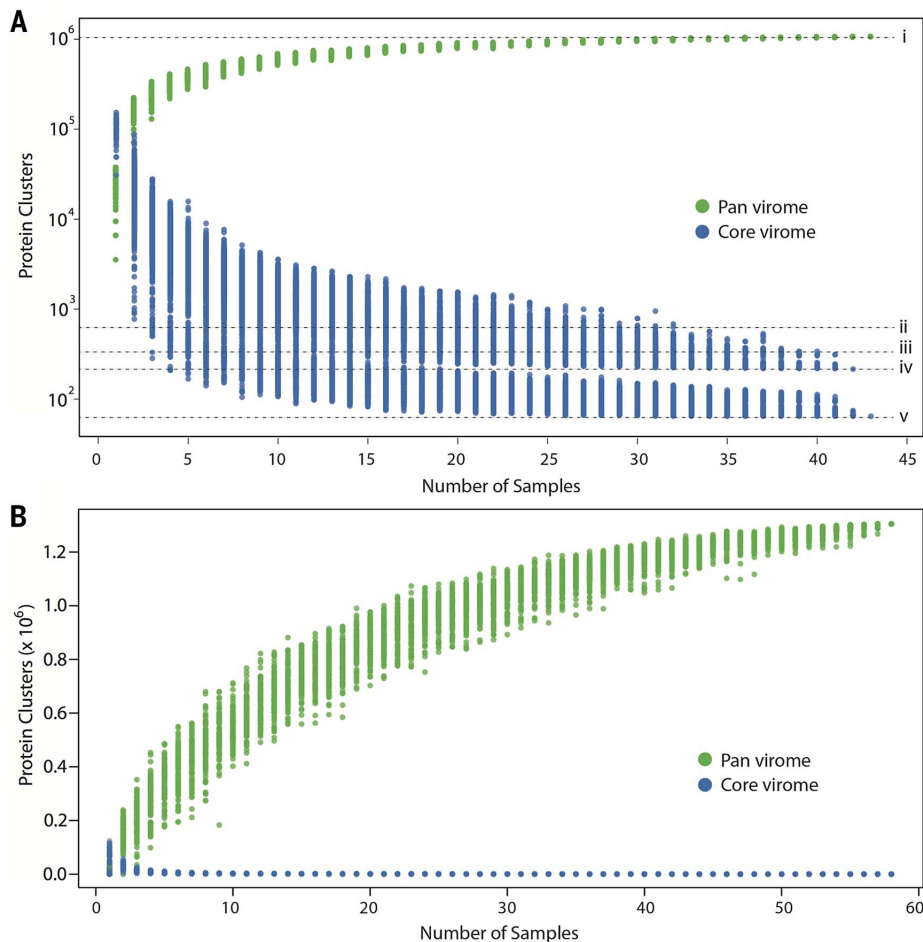


Fig. 2. PC richness in core and pan viromes from the TOV and POV data sets. (A) Accumulation curves of core and pan PCs in the TOV data set. Vertical axis shows the number of shared (core virome) and total (pan virome) PCs when n viromes are compared ($n = 1$ to 43; from 3 to 41 only 1000 combinations are shown). Lines: (i) total number of PCs (1,075,763 PCs), (ii) core surface virome (710 PCs), (iii) core DCM virome (424 PCs), (iv) core surface and DCM virome (220 PCs), (v) all samples (including the deep-ocean sample TARA_70_MESO; 65 PCs). **(B)** Core and pan PCs in all TOV and photic-zone POV samples combined. Vertical axis shows the number of shared (core virome) and total (pan-virome) PCs when n viromes are compared ($n = 1$ to 58; from 3 to 58 only 1000 combinations are shown). Overall, 1,323,921 PCs were identified in all viromes combined.

Until methods to link viruses to their host cells in natural communities mature to the point of investigating this issue at larger scales [emerging possible methods reviewed by (33, 45)], analyses such as ours remain the only means to assess ecological drivers of viral community structure.

To further investigate how ocean viral communities are distributed throughout the oceans, we compared population abundances between neighboring samples to assess the net direction and magnitude of population exchange (Fig. 7 and see Methods). These genomic signals revealed that population exchange between dsDNA viral communities was largely directed along major oceanic current systems (46). For example, the Agulhas current and subsequent ring formation (47) connects viral communities between the

Indian and Atlantic Oceans, as also observed in planktonic communities from the *Tara* Oceans expedition (48), whereas increased connection between the high-latitude stations (TARA_82 and TARA_85) reflects their common origin at the divergence of the Falklands and Antarctic Circumpolar currents. Further, current strength (46) was generally related to the magnitude of intersample population exchange, as higher and lower exchange was observed, respectively, in stronger currents, such as the Agulhas current, and within the open ocean gyres or between land-restricted basins such as the Mediterranean and Red Seas. These findings suggest that the intensity of water mass movement, in addition to environmental conditions, may explain the degree to which viral populations cluster globally (Fig. 4). Beyond such current-driven biogeographic

evidence, vertical viral transport from surface to DCM samples was also observed (Fig. 4). This is consistent with POV observations wherein deep-sea viromes include a modest influx of genetic material derived from surface-ocean viruses that are presumably transported on sinking particles (28). Exceptions include areas such as the Arabian Sea upwelling region, where increased mixing and upwelling likely exceed sinking within the upper ocean.

Our TOV results enabled evaluation of a hypothesis describing the structure of viral communities in the environment. Gene marker-based studies targeting subsets of ocean viruses previously found high local and low global diversity (49), a pattern also recently observed genome-wide in natural cyanophage populations (11). To explain this, a seed-bank viral community structure has been invoked, whereby high local genetic diversity can exist by drawing variation from a common and relatively limited global gene pool (49). Our results support this hypothesis regarding viral community structure. Ecological driver analyses suggests that the numerically dominant members in local communities are influenced by environmental conditions, which directly impact their microbial hosts and then indirectly restructure viral communities. These dominant communities then form the “bank” in neighboring samples, presumably when passively transported by ocean currents as shown here through the population-level analyses of net viral movement between samples. This systematically sampled global data set suggests that large- and small-scale processes play roles in structuring viral communities and offers empirical grounding for the seed-bank hypothesis with regard to viral community distribution and structure.

Conclusions

Our large-scale data set provides a picture of global upper-ocean viral communities in which we assessed patterns using multiple parameters, including morphology, populations, and PCs. Our data provide advanced and complementary views on viral community structure including diversity estimates not based on marker genes and broad application of population-based viral ecology. We affirm the seed-bank model for viruses, hypothesized nearly a decade ago (49), which explains how high local viral diversity can be consistent with limited global diversity (11, 27). The mechanism underlying this seed-bank population structure appears to be a local production of viruses under small-scale environmental constraints and passive dispersal with oceanic currents. Improving sequencing, assembly, and experimental methods are transforming the investigation of viruses in nature (33, 45) and pave the way toward assessment of viral community structure and analysis of virus-host co-occurrence networks (50) without requiring marker genes (51, 52). Such experimental and analytical progress, coupled to sampling opportunities from the *Tara* Oceans expedition, are advancing viral ecology toward the quantitative science needed to model the nanoscale

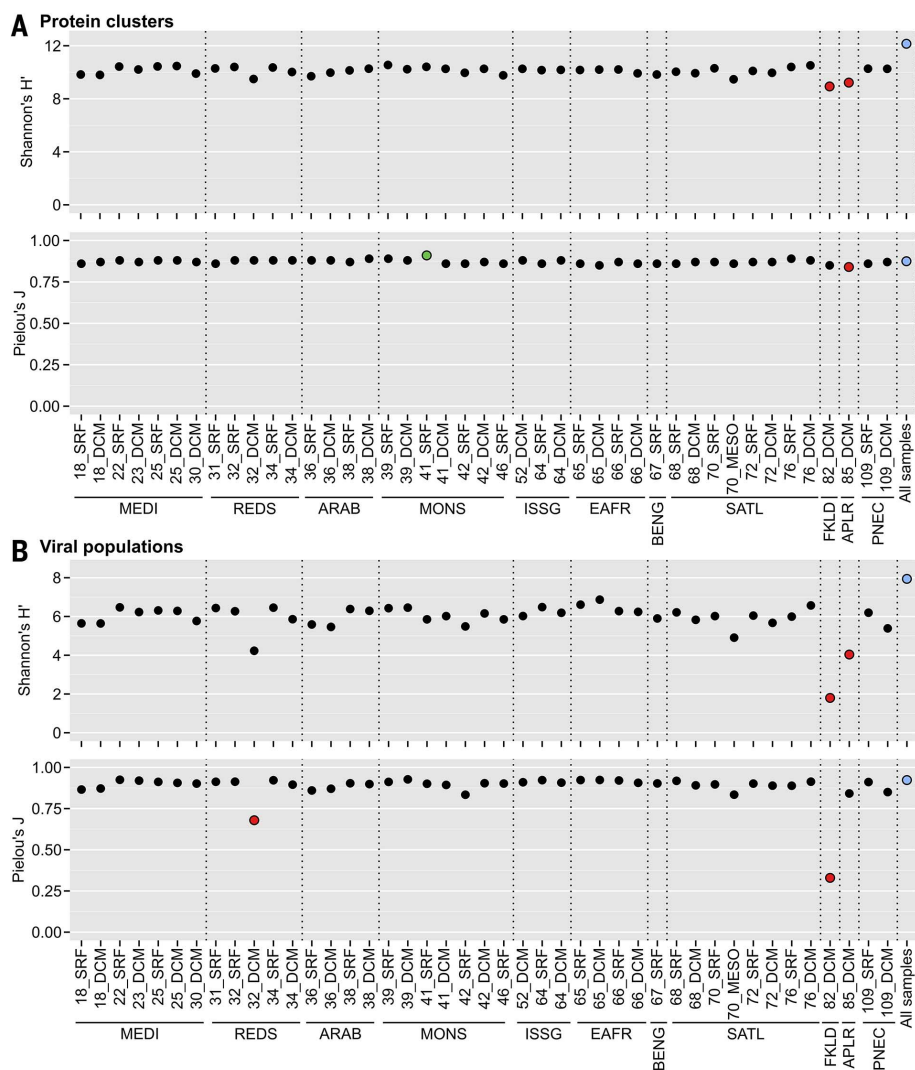


Fig. 3. Alpha diversity measurements in TOV data set. (A) Shannon's diversity H' and Pielou's evenness J calculated from protein cluster counts for each sample and a pool of all samples, normalized to 5 million reads. (B) Shannon's diversity H' and Pielou's evenness J calculated from relative abundances of viral populations for each sample and a pool of all samples, with subsamples of 100,000 reads. Outliers corresponding to values outside of the average value ± 2 SD are colored green and red, respectively. Values calculated from the pool of all samples are colored blue. Longhurst provinces are indicated below samples using the same abbreviations as in Fig. 1.

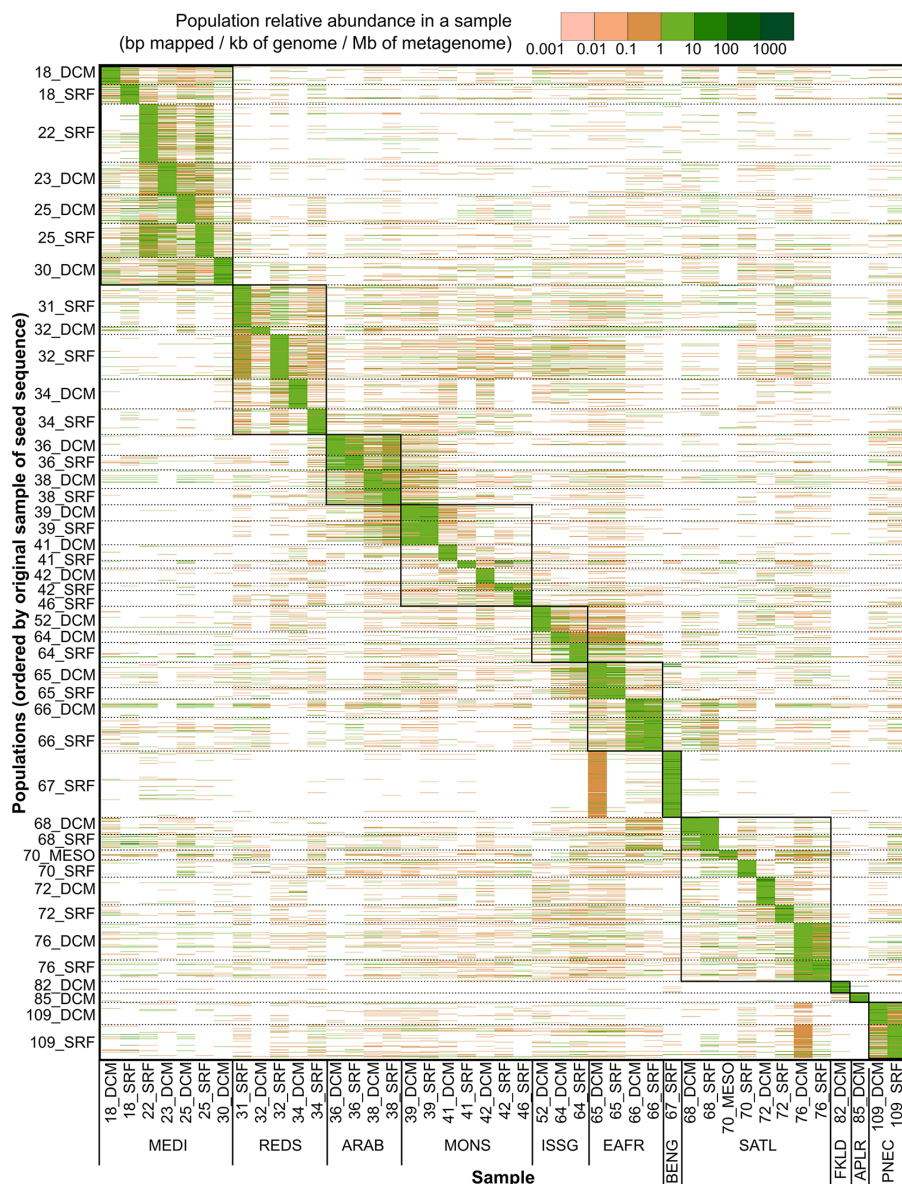


Fig. 4. Relative abundance of viral populations in TOV by sample. This heat map displays the relative abundance of each population (sorted according to its original sample, y axis) in each sample (x axis). Relative abundance of one population in a sample is based on recruitment of reads to the population reference contig and is only considered if more than 75% of the reference contig is covered. Longhurst provinces are indicated below samples (using the same abbreviations as in Fig. 1) and are outlined in black on the heat map.

(viruses) and microscale (microbes) entities driving Earth's ecosystems.

Materials and methods

Sample collection

Forty-three samples were collected between 2 November 2009 and 13 May 2011, at 26 locations throughout the world's oceans (file S1) through the *Tara* Oceans Expedition (5). These included samples from a range of depths (surface, deep chlorophyll maximum, and one mesopelagic sample) located in seven oceans and seas, four different biomes, and 11 Longhurst oceanographic provinces (file S1). Longhurst provinces and biomes are defined based on Longhurst (53) and environmental features are defined based on En-

vironment Ontology (<http://environmentontology.org/>). Sampling strategy and methodology for the *Tara* Oceans Expedition is fully described by Pesant *et al.* (54).

Environmental parameters

Temperature, salinity, and oxygen data were collected from each station by measuring conductivity, temperature, depth, and pressure using a CTD (Sea-Bird Electronics, Bellevue, WA, USA; SBE 911plus with Searam recorder) and with a dissolved oxygen sensor (Sea-Bird Electronics; SBE 43). Nutrient concentrations were determined using segmented flow analysis (55) and included nitrite, phosphate, nitrite plus nitrate, and silica. Nutrient concentrations below the

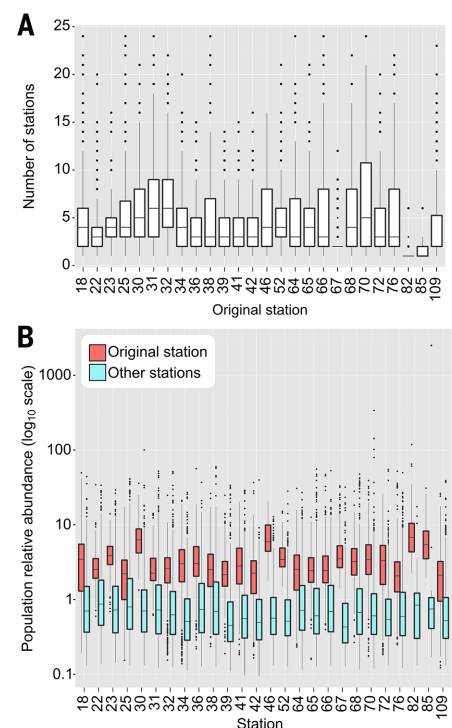


Fig. 5. Relative abundance of viral populations in TOV by station. (A) Evaluation of viral population distribution showing the number of stations (y axis) in which each population (sorted by their original station, x axis) is distributed. Populations are grouped by station, merging surface, and DCM samples from the same station. (B) Relative abundance of populations (bp mapped per Kb of contig per Mb of metagenome) at the original stations where the contigs were assembled compared with their abundance at other stations. Box plots are constructed as in Fig. 1.

detection limit ($0.02 \mu\text{mol kg}^{-1}$) are reported as $0.02 \mu\text{mol kg}^{-1}$. Chlorophyll concentrations were measured using high-performance liquid chromatography (56, 57). These environmental parameters are available in PANGAEA (www.pangaea.de) by using the accession numbers in file S1.

Microbial abundances

Flow cytometry was used to determine the concentration of *Synechococcus*, *Prochlorococcus*, total bacteria, low-DNA bacteria, high-DNA bacteria, and the percentage of bacteria with high DNA in each sample (58).

Morphological analysis of viral communities

qTEM was used to evaluate the capsid diameter distributions of viral communities as previously described (7). Briefly, preserved unfiltered samples (electron microscopy-grade glutaraldehyde; Sigma-Aldrich, St. Louis, MO, USA; 2% final concentration) were flash-frozen and stored at -80°C until analysis. Viruses were deposited onto TEM grids using an air-driven ultracentrifuge (Airfuge CLS, Beckman Coulter, Brea, CA, USA), followed

by positive staining of the deposited material with 2% uranyl acetate (Ted Pella, Redding, CA, USA). Samples were then examined by using a transmission electron microscope (Philips CM12 FEI, Hillsboro, OR, USA) with 100 kV accelerating voltage. Micrographs of 100 viruses were collected per sample using a Macrofire Monochrome charge-coupled device camera (Optronics, Goleta, CA, USA) and analyzed using ImageJ software (U.S. National Institutes of Health, Bethesda, MD, USA) (59) to measure the capsid diameter. A subset (21) of the 41 samples presented here had previously been analyzed in a different study (7).

Virome construction

For each sample, 20 L of seawater were 0.22- μ m-filtered, and viruses were concentrated from the filtrate using iron chloride flocculation (15) followed by storage at 4°C. After resuspension in ascorbic-EDTA buffer (0.1 M EDTA, 0.2 M Mg, 0.2 M ascorbic acid, pH 6.0), viral particles were concentrated using Amicon Ultra 100-kD centrifugal devices (Millipore), treated with DNase I (100 U/mL) followed by the addition of 0.1 M EDTA and 0.1 M EGTA to halt enzyme activity, and extracted as previously described (14). Briefly, viral particle suspensions were treated with Wizard Polymerase Chain Reaction Preps DNA Purification Resin (Promega, Fitchburg, WI, USA) at a ratio of 0.5-ml sample to 1-ml resin, and eluted with TE buffer (10 mM Tris, pH 7.5, 1 mM EDTA) using Wizard Minicolumns. Extracted DNA was Covaris-sheared and size-selected to 160 to 180 bp, followed by amplification and ligation per the standard Illumina protocol.

Sequencing was done on a HiSeq 2000 system at the Genoscope facilities (Paris, France).

Quality control of reads and assembly

Individual reads of 43 metagenomes were controlled for quality by using a combination of trimming and filtering as previously described (60). Briefly, bases were trimmed at the 5' end if the number of base calls for any base (A, T, G, C) diverged by more than 2 SD from the average across all cycles. Conversely, bases were trimmed at the 3' end of reads if the quality score was <20. Finally, reads that were shorter than 95 bp or reads with a median quality score <20 were removed from further analyses. Assembly of reads was done using SOAPdenovo (61), where insert and *k*-mer size are calculated at runtime and are specific to each virome as implemented in the MOCAT pipeline (62). On average, 34.2% of the virome reads were included in the assembled contigs (min: 21.08%, max: 48.52%). Virome reads were deposited in the European Nucleotide Archive (www.ebi.ac.uk/ena/) under accession numbers reported in file S1.

Protein clustering

Open reading frames (ORFs) were predicted from all quality-controlled contigs using Prodigal (63) with default settings. Predicted ORFs were clustered on the basis of sequence similarity as described previously (9, 10). Briefly, ORFs were initially mapped to existing clusters [POV, Global Ocean Sampling expedition, and phage genomes], by using cd-hit-2d ("g 1-n 4-d 0-T 24-M 45000"; 60% identity and 80% coverage). Then, the re-

maining, unmapped ORFs were self-clustered, using cd-hit with the same options as above. Only PCs with more than two ORFs were considered bona fide and were used for subsequent analyses. To develop read counts per PC for statistical analyses, reads were mapped back to predicted ORFs in the contigs data set using Mosaik with the following settings: "-a all -m all -hs 15 -minp 0.95 -mmp 0.05 -mhp 100 -act 20" (version 1.1.0021; <http://bioinformatics.bc.edu/mathlab/Mosaik>). Read counts to PCs were normalized by sequencing depth of each virome. Shannon's diversity index (*H'*) was calculated from PC read counts by using only PCs with more than two predicted ORFs. Observed richness is reported as the total number of reads in each PC. Pielou's evenness (*J*) was calculated as the ratio of H'/H_{\max} , where $H_{\max} = \ln N$, and N = total number of observed PCs in a sample.

Analysis of viral populations

Considering the size of the entire data set (3,821,756 assembled contigs), we decided to focus the analysis of viral populations using contigs originating from bacterial or archaeal viruses. For this, we mined only the 22,912 contigs with more than 10 predicted genes (corresponding to an average of 6.41% of the assembled reads per sample, min: 1.29%, max: 14.52%), as the origin of contigs with only a few predicted genes can be spurious. First, we removed 6706 contigs suspected of having originated from cellular genomes (64), whether due to free genomic DNA contamination or viral-encapsulation of cellular DNA (for example, in gene transfer agents or generalized transducing phages). These suspect cellular contigs were those containing no typical viral genes (such as virion-related genes including major capsid proteins and large subunits of the terminase) and displaying as many genes with a significant similarity to a PFAM domain through Hmmsrch (65) as a typical cellular genome, whereas phage genomes are typically enriched in uncharacterized genes (40). We also removed all contigs posited to originate from eukaryotic viruses. These were contigs that contained at least three predicted proteins with best BLAST hits to a eukaryotic virus, and more than half of the affiliated proteins were not associated with bacteriophages or archaeal viruses. Not surprisingly, given that eukaryotes are outnumbered by bacteria and archaea in the marine environment, this step removed only 142 contigs associated with eukaryotic viruses. From the remaining 16,124 contigs most likely to have originated from bacterial or archaeal viruses, the population study only used those longer than 10 kb in size—a total of 6322 contigs, which corresponded to an average of 4.04% of the assembled reads per sample (min: 0.98%, max: 9.97%).

These 6322 contigs were then clustered into populations if they shared more than 80% of their genes at >95% nucleotide identity; a threshold derived from naturally occurring T4-like cyanophages (11). This resulted in 5476 populations from the 6322 contigs, where as many

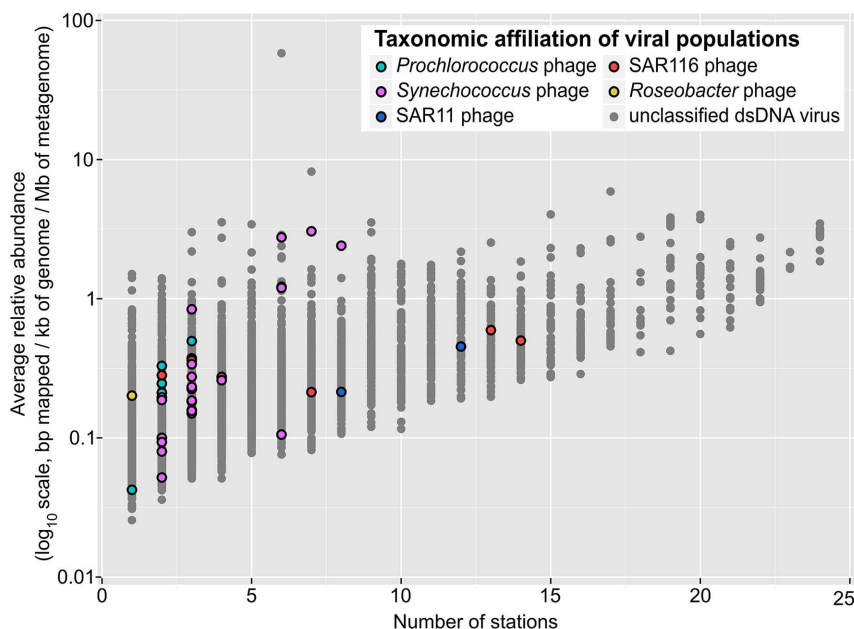


Fig. 6. Taxonomic affiliation of TOV viral populations sorted by distribution and average abundance.

A population was considered as similar to a known virus when fewer than half of its reference contig genes were uncharacterized, and all characterized genes had taxonomic affiliations to the same reference genome. As in Fig. 4, the relative abundance (*y* axis) is computed for each sample as the number of bp mapped to a contig per kb of contig per Mb of metagenome sequenced. Here, the relative abundance of a population is defined as the average abundance of its reference contig across all samples.

Table 1. Relations between viral community structure and metadata. Relations between viral community structure (based on viral morphology, populations, and PCs) and metadata by using NMDS analysis of all samples and the sample subset (all samples except for TARA_67_SRF, TARA_70_MESO, TARA_82_DCM, and TARA_85_DCM because of exceptional environmental conditions at these locations). Significant relations are bold.

Category	N and n	Viral morphology (qTEM)	Populations (contigs)	Protein clusters (PCs)
Depth category	All samples	$P = 0.354$ ($N = 41$)	$P = 0.362$ ($N = 43$)	$P = 0.033$ ($N = 43$)
	Sample subset	$P = 0.228$ ($n = 38$)	$P = 0.105$ ($n = 39$)	$P = 0.011$ ($n = 39$)
Province	All samples	$P = 0.098$ ($N = 41$)	$P < 0.001$ ($N = 43$)	$P = 0.014$ ($N = 43$)
	Sample subset	$P = 0.029$ ($n = 38$)	$P < 0.001$ ($n = 39$)	$P = 0.008$ ($n = 39$)
Biome	All samples	$P = 0.099$ ($N = 41$)	$P < 0.001$ ($N = 43$)	$P = 0.097$ ($N = 43$)
	Sample subset	$P = 0.120$ ($n = 38$)	$P < 0.001$ ($n = 39$)	$P = 0.543$ ($n = 39$)
Latitude	All samples	$P = 0.003$ ($N = 41$)	$P < 0.001$ ($N = 43$)	$P = 0.002$ ($N = 43$)
	Sample subset	$P = 0.014$ ($n = 38$)	$P < 0.001$ ($n = 39$)	$P = 0.010$ ($n = 39$)
Temperature	All samples	$P = 0.001$ ($N = 41$)	$P < 0.001$ ($N = 43$)	$P < 0.001$ ($N = 43$)
	Sample subset	$P = 0.001$ ($n = 38$)	$P < 0.001$ ($n = 39$)	$P = 0.015$ ($n = 39$)
Salinity	All samples	$P = 0.118$ ($N = 39$)	$P = 0.035$ ($N = 41$)	$P = 0.029$ ($N = 41$)
	Sample subset	$P = 0.138$ ($n = 36$)	$P = 0.075$ ($n = 37$)	$P = 0.001$ ($n = 37$)
Oxygen	All samples	$P = 0.001$ ($N = 41$)	$P < 0.001$ ($N = 43$)	$P < 0.001$ ($N = 43$)
	Sample subset	$P = 0.005$ ($n = 38$)	$P < 0.001$ ($n = 39$)	$P < 0.001$ ($n = 39$)
Chlorophyll	All samples	$P = 0.711$ ($N = 41$)	$P < 0.001$ ($N = 43$)	$P = 0.001$ ($N = 39$)
	Sample subset	$P = 0.738$ ($n = 38$)	$P = 0.412$ ($n = 39$)	$P = 0.059$ ($n = 39$)
Nitrite	All samples	$P = 0.951$ ($N = 39$)	$P = 0.648$ ($N = 41$)	$P = 0.828$ ($N = 41$)
	Sample subset	$P = 0.851$ ($n = 36$)	$P = 0.509$ ($n = 37$)	$P = 0.999$ ($n = 37$)
Phosphate	All samples	$P = 0.275$ ($N = 39$)	$P < 0.001$ ($N = 41$)	$P < 0.001$ ($N = 41$)
	Sample subset	$P = 0.411$ ($n = 36$)	$P < 0.001$ ($n = 37$)	$P = 0.583$ ($n = 37$)
Nitrite + Nitrate	All samples	$P = 0.046$ ($N = 39$)	$P < 0.001$ ($N = 41$)	$P < 0.001$ ($N = 41$)
	Sample subset	$P = 0.290$ ($n = 36$)	$P = 0.052$ ($n = 37$)	$P = 0.643$ ($n = 37$)
Silica	All samples	$P = 0.008$ ($N = 39$)	$P = 0.002$ ($N = 41$)	$P = 0.008$ ($N = 41$)
	Sample subset	$P = 0.255$ ($n = 36$)	$P = 0.285$ ($n = 37$)	$P = 0.191$ ($n = 37$)
Bacteria	All samples	$P = 0.579$ ($N = 39$)	$P < 0.001$ ($N = 40$)	$P = 0.119$ ($N = 40$)
	Sample subset	$P = 0.329$ ($n = 36$)	$P = 0.003$ ($n = 36$)	$P = 0.007$ ($n = 36$)
Low DNA bacteria	All samples	$P = 0.227$ ($N = 39$)	$P = 0.090$ ($N = 40$)	$P = 0.123$ ($N = 40$)
	Sample subset	$P = 0.468$ ($n = 36$)	$P = 0.018$ ($n = 36$)	$P = 0.005$ ($n = 36$)
High DNA bacteria	All samples	$P = 0.967$ ($N = 39$)	$P < 0.001$ ($N = 40$)	$P = 0.273$ ($N = 40$)
	Sample subset	$P = 0.174$ ($n = 36$)	$P = 0.027$ ($n = 36$)	$P = 0.024$ ($n = 36$)
Percentage of high-DNA bacteria	All samples	$P = 0.007$ ($N = 39$)	$P = 0.078$ ($N = 40$)	$P = 0.009$ ($N = 40$)
	Sample subset	$P = 0.017$ ($n = 36$)	$P = 0.059$ ($n = 36$)	$P < 0.001$ ($n = 36$)
<i>Synechococcus</i>	All samples	$P = 0.143$ ($N = 39$)	$P = 0.094$ ($N = 40$)	$P = 0.041$ ($N = 40$)
	Sample subset	$P = 0.142$ ($n = 36$)	$P = 0.023$ ($n = 36$)	$P = 0.013$ ($n = 36$)
<i>Prochlorococcus</i>	All samples	$P = 0.118$ ($N = 39$)	$P = 0.076$ ($N = 40$)	$P = 0.123$ ($N = 40$)
	Sample subset	$P = 0.249$ ($n = 37$)	$P = 0.161$ ($n = 37$)	$P = 0.140$ ($n = 37$)

as 12 contigs (average 1.15 contigs) were included per population. For each population, the longest contig was chosen as the seed sequence.

The relative abundance of each population was computed by mapping all quality-controlled reads to the set of 5476 nonredundant populations (considering only mapping quality scores greater than 1) with Bowtie 2 (66). For each sample-sequence pair, if more than 75% of the reference sequence was covered by virome reads, the relative abundance was computed as the number of base pairs recruited to the contig normalized to the total number of base pairs available in the virome and the contig length. Shannon diversity index (H') and Pielou's evenness (J) were calculated as done for PCs using the relative abundance of viral populations.

The sample containing the seed sequence (the longest contig in a population) was also considered the best estimate of that population's origin. We reasoned that this was because the

longest contig in a population would derive most often from the sample with the highest coverage (a proxy for population abundance) and likely corresponded to the location with the greatest viral abundance for this population. This assumption was supported by the results showing that populations were most abundant in their original samples (Figs. 4 and 5B). Even though some individual cases could diverge from this rule, we expected to correctly identify most of these original locations and, hence, to get an accurate global signal.

The seed sequence was also used to assess taxonomic affiliation of the viral population. Cases where >50% of the genes were affiliated to a specific reference genome from RefSeq (based on a BLASTp comparison with thresholds of 50 for bit score and 10^{-5} for e-value) with an identity percentage of at least 75% (at the protein sequence level) were considered confident affiliations with the corresponding reference virus.

Finally, estimations of net viral population movement between samples were made on the basis of the relative abundance of populations in one sample compared with that of its neighboring samples (Fig. 4). For each neighboring sample pair, the average relative abundance of populations originating from sample A in sample B was compared with the relative abundance of populations originating from sample B in sample A. The origin of each population was defined as the sample in which the longest contig of the population was assembled. The magnitude of these differences was carried through the analysis to estimate the level of transport between each pair of samples (depicted as line width in Fig. 7) and the difference between these values was used to estimate the directionality of the transfer. For example, if sample B contains many populations from sample A, but very few populations from sample B are detected in sample A, we calculate that the net movement

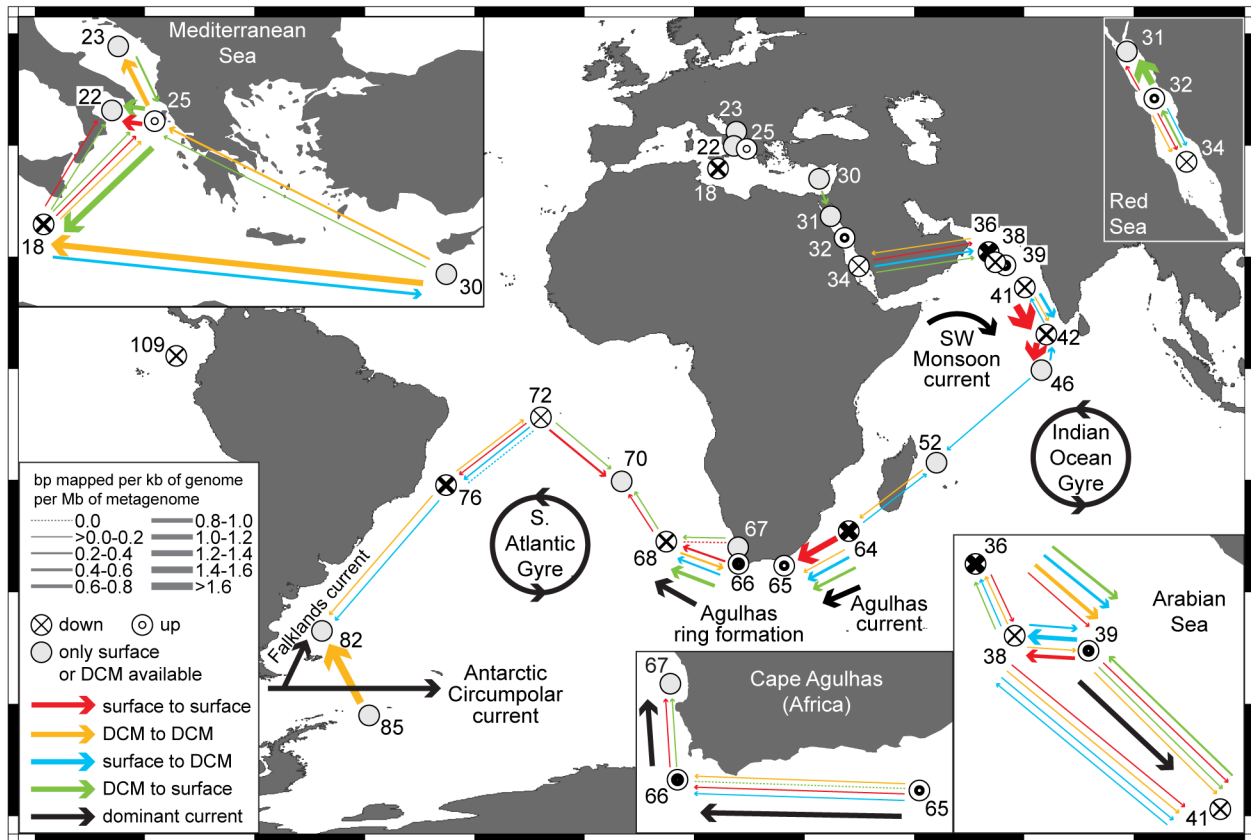


Fig. 7. Net movement of viral populations throughout the oceans. Calculations are based on reciprocal comparison of viral population abundances between neighboring samples (see Fig. 3 and Methods). For each sample pair, the average relative population abundances in one sample originating from a neighboring sample were calculated and compared (for example, relative abundance of populations from sample A found in sample B are compared with relative abundance

of populations from sample B found in sample A). The sign of the relative abundance difference between neighboring samples was used to estimate the movement direction (arrowhead) and the absolute value of the difference was interpreted as reflecting the movement magnitude (line width). Stations are labeled with station number. “Down” and “up” refer to net vertical movement of viral populations between the surface and DCM samples at the same station.

is from sample A to sample B. Again, although the sampling of some populations may not be strong, the net movement was calculated as the average of all shared populations between neighboring sample pairs, which corresponded to 105 different populations on average (ranging from 2 to 412).

Statistical ordination of samples

Viral community composition based on capsid diameter distributions (from qTEM; using 7-nm histogram bin sizes), population abundances, and normalized PC read counts (using only PCs with more than 20 representatives) were compared by using nonmetric multidimensional scaling (NMDS) performed using the “metaMDS” function (default parameters) of the vegan package (67) in R version 2.15.2 (68). The influence of metadata on sample ordination was evaluated using the functions in the vegan package “envfit”—for factor variables including depth category, Longhurst province, and biome—and “ordisurf” for all linear variables (67, 69). Several samples had exceptional environmental conditions (TARA_67_SUR, TARA_70_MESO, TARA_82_DCM, and TARA_85_DCM), thus all statistical ordination analyses were conducted with

and without these samples (referred to as the “sample subset”) to evaluate their influence.

REFERENCES AND NOTES

- C. B. Field, M. J. Behrenfeld, J. T. Randerson, P. Falkowski, Primary production of the biosphere: Integrating terrestrial and oceanic components. *Science* **281**, 237–240 (1998). doi: [10.1126/science.281.5374.237](https://doi.org/10.1126/science.281.5374.237); pmid: 9657713
- P. G. Falkowski, T. Fenchel, E. F. Delong, The microbial engines that drive Earth’s biogeochemical cycles. *Science* **320**, 1034–1039 (2008). doi: [10.1126/science.1153213](https://doi.org/10.1126/science.1153213); pmid: 18497287
- M. Breitbart, Marine viruses: Truth or dare. *Annu. Rev. Mar. Sci.* **4**, 425–448 (2012). doi: [10.1146/annurev-marine-120709-142805](https://doi.org/10.1146/annurev-marine-120709-142805); pmid: 22457982
- C. A. Suttle, Marine viruses—major players in the global ecosystem. *Nat. Rev. Microbiol.* **5**, 801–812 (2007). doi: [10.1038/nrmicro1750](https://doi.org/10.1038/nrmicro1750); pmid: 17853907
- E. Karsenti et al., A holistic approach to marine eco-systems biology. *PLOS Biol.* **9**, e1001177 (2011). doi: [10.1371/journal.pbio.1001177](https://doi.org/10.1371/journal.pbio.1001177); pmid: 22028628
- S. A. Solonenko et al., Sequencing platform and library preparation choices impact viral metagenomes. *BMC Genomics* **14**, 320 (2013). doi: [10.1186/1471-2164-14-320](https://doi.org/10.1186/1471-2164-14-320); pmid: 23663384
- J. R. Brum, R. O. Schenck, M. B. Sullivan, Global morphological analysis of marine viruses shows minimal regional variation and dominance of non-tailed viruses. *ISME J.* **7**, 1738–1751 (2013). doi: [10.1038/ismej.2013.67](https://doi.org/10.1038/ismej.2013.67); pmid: 23635867
- P. Hingamp et al., Exploring nucleocytoplasmic large DNA viruses in Tara Oceans microbial metagenomes. *ISME J.* **7**, 1678–1695 (2013). doi: [10.1038/ismej.2013.59](https://doi.org/10.1038/ismej.2013.59); pmid: 23575371
- S. Yooseph et al., The Sorcerer II Global Ocean Sampling expedition: Expanding the universe of protein families. *PLOS Biol.* **5**, e16 (2007). pmid: 17355171
- B. L. Hurwitz, M. B. Sullivan, The Pacific Ocean virome (POV): A marine viral metagenomic dataset and associated protein clusters for quantitative viral ecology. *PLOS ONE* **8**, e57355 (2013). doi: [10.1371/journal.pone.0057355](https://doi.org/10.1371/journal.pone.0057355); pmid: 23468974
- L. Deng et al., Viral tagging reveals discrete populations in *Synechococcus* viral genome sequence space. *Nature* **513**, 242–245 (2014). doi: [10.1038/nature13459](https://doi.org/10.1038/nature13459); pmid: 25043051
- M. B. Duhaime, M. B. Sullivan, Ocean viruses: Rigorously evaluating the metagenomic sample-to-sequence pipeline. *Virology* **434**, 181–186 (2012). doi: [10.1016/j.virol.2012.09.036](https://doi.org/10.1016/j.virol.2012.09.036); pmid: 23084423
- M. B. Duhaime, L. Deng, B. T. Poulos, M. B. Sullivan, Towards quantitative metagenomics of wild viruses and other ultra-low concentration DNA samples: A rigorous assessment and optimization of the linker amplification method. *Environ. Microbiol.* **14**, 2526–2537 (2012). doi: [10.1111/j.1462-2920.2012.02791.x](https://doi.org/10.1111/j.1462-2920.2012.02791.x); pmid: 22713159
- B. L. Hurwitz, L. Deng, B. T. Poulos, M. B. Sullivan, Evaluation of methods to concentrate and purify ocean virus communities through comparative, replicated metagenomics. *Environ. Microbiol.* **15**, 1428–1440 (2013). doi: [10.1111/j.1462-2920.2012.02836.x](https://doi.org/10.1111/j.1462-2920.2012.02836.x); pmid: 22845467
- S. G. John et al., A simple and efficient method for concentration of ocean viruses by chemical flocculation. *Environ. Microbiol. Rep.* **3**, 195–202 (2011). doi: [10.1111/j.1758-2229.2010.00208.x](https://doi.org/10.1111/j.1758-2229.2010.00208.x); pmid: 21572525
- G. F. Steward et al., Are we missing half of the viruses in the ocean? *ISME J.* **7**, 672–679 (2013). doi: [10.1038/ismej.2012.121](https://doi.org/10.1038/ismej.2012.121); pmid: 23151645

17. K. Holmfeldt, D. Odić, M. B. Sullivan, M. Middelboe, L. Riemann, Cultivated single-stranded DNA phages that infect marine Bacteroidetes prove difficult to detect with DNA-binding stains. *Appl. Environ. Microbiol.* **78**, 892–894 (2012). doi: [10.1128/AEM.06580-11](https://doi.org/10.1128/AEM.06580-11); pmid: 22138992
18. Y. Tomaru, K. Nagasaki, Flow cytometric detection and enumeration of DNA and RNA viruses infecting marine eukaryotic microalgae. *J. Oceanogr.* **63**, 215–221 (2007). doi: [10.1007/s10872-007-0023-8](https://doi.org/10.1007/s10872-007-0023-8)
19. C. P. D. Brussaard, D. Marie, G. Bratbak, Flow cytometric detection of viruses. *J. Virol. Methods* **85**, 175–182 (2000). doi: [10.1016/S0166-0934\(99\)00167-6](https://doi.org/10.1016/S0166-0934(99)00167-6); pmid: 10716350
20. Y. Bettarel, T. Sime-Ngando, C. Amblard, H. Laveran, A comparison of methods for counting viruses in aquatic systems. *Appl. Environ. Microbiol.* **66**, 2283–2289 (2000). doi: [10.1128/AEM.66.6.2283-2289.2000](https://doi.org/10.1128/AEM.66.6.2283-2289.2000); pmid: 10831400
21. K. P. Hennes, C. A. Suttle, Direct counts of viruses in natural waters and laboratory cultures by epifluorescence microscopy. *Limnol. Oceanogr.* **40**, 1050–1055 (1995). doi: [10.4319/lo.1995.40.6.1050](https://doi.org/10.4319/lo.1995.40.6.1050)
22. M. G. Weinbauer, C. A. Suttle, Comparison of epifluorescence and transmission electron microscopy for counting viruses in natural marine waters. *Aquat. Microb. Ecol.* **13**, 225–232 (1997). doi: [10.3354/ame013225](https://doi.org/10.3354/ame013225)
23. R. T. Noble, J. A. Fuhrman, Use of SYBR Green I for rapid epifluorescence counts of marine viruses and bacteria. *Aquat. Microb. Ecol.* **14**, 113–118 (1998). doi: [10.3354/ame014113](https://doi.org/10.3354/ame014113)
24. D. Marie, C. P. D. Brussaard, R. Thyrhaug, G. Bratbak, D. Vaulot, Enumeration of marine viruses in culture and natural samples by flow cytometry. *Appl. Environ. Microbiol.* **65**, 45–52 (1999). pmid: 9872758
25. S. Sunagawa, Structure and function of the global ocean microbiome. *Science* **348**, 1261359 (2015).
26. D. M. Kristensen *et al.*, Orthologous gene clusters and taxon signature genes for viruses of prokaryotes. *J. Bacteriol.* **195**, 941–950 (2013). doi: [10.1128/JB.01801-12](https://doi.org/10.1128/JB.01801-12); pmid: 23222723
27. J. C. Ignacio-Espinoza, S. A. Solonenko, M. B. Sullivan, The global virome: Not as big as we thought? *Curr. Opin. Virol.* **3**, 566–571 (2013). doi: [10.1016/j.coviro.2013.07.004](https://doi.org/10.1016/j.coviro.2013.07.004); pmid: 23896279
28. B. L. Hurwitz, J. R. Brum, M. B. Sullivan, Depth-stratified functional and taxonomic niche specialization in the ‘core’ and ‘flexible’ Pacific Ocean Virome. *ISME J.* **9**, 472–484 (2015). doi: [10.1038/ismej.2014.143](https://doi.org/10.1038/ismej.2014.143); pmid: 25093636
29. D. P. Tittensor *et al.*, Global patterns and predictors of marine biodiversity across taxa. *Nature* **466**, 1098–1101 (2010). doi: [10.1038/nature09329](https://doi.org/10.1038/nature09329); pmid: 20668450
30. W. J. Sul, T. A. Oliver, H. W. Ducklow, L. A. Amaral-Zettler, M. L. Sogin, Marine bacteria exhibit a bipolar distribution. *Proc. Natl. Acad. Sci. U.S.A.* **110**, 2342–2347 (2013). doi: [10.1073/pnas.1212424110](https://doi.org/10.1073/pnas.1212424110); pmid: 23324742
31. D. I. Jarvis *et al.*, A global perspective of the richness and evenness of traditional crop-variety diversity maintained by farming communities. *Proc. Natl. Acad. Sci. U.S.A.* **105**, 5326–5331 (2008). doi: [10.1073/pnas.0800607105](https://doi.org/10.1073/pnas.0800607105); pmid: 18362337
32. S. P. Hubbell, *The Unified Neutral Theory of Biodiversity and Biogeography* (Princeton Univ. Press, Princeton, NJ, 2001).
33. J. R. Brum, M. B. Sullivan, Rising to the challenge: Accelerated pace of discovery transforms marine virology. *Nat. Rev. Microbiol.* **13**, 147–159 (2015). doi: [10.1038/nrmicro3404](https://doi.org/10.1038/nrmicro3404); pmid: 25639680
34. C. de Vargas *et al.*, Global oceans eukaryotic plankton diversity. *Science* **348**, 1261605 (2015).
35. I. Kang, H.-M. Oh, D. Kang, J.-C. Cho, Genome of a SAR116 bacteriophage shows the prevalence of this phage type in the oceans. *Proc. Natl. Acad. Sci. U.S.A.* **110**, 12343–12348 (2013). doi: [10.1073/pnas.1219930110](https://doi.org/10.1073/pnas.1219930110); pmid: 23798439
36. S. J. Labrie *et al.*, Genomes of marine cyanobacteriophages reveal multiple origins of diversity. *Environ. Microbiol.* **15**, 1356–1376 (2013). doi: [10.1111/1462-2920.12053](https://doi.org/10.1111/1462-2920.12053); pmid: 23320838
37. M. B. Sullivan *et al.*, Genomic analysis of ocean cyanobacterial myoviruses compared with T4-like myoviruses from diverse hosts and environments. *Environ. Microbiol.* **12**, 3035–3056 (2010). doi: [10.1111/j.1462-2920.2010.02280.x](https://doi.org/10.1111/j.1462-2920.2010.02280.x); pmid: 20662890
38. Y. Zhao *et al.*, Abundant SAR11 viruses in the ocean. *Nature* **494**, 357–360 (2013). doi: [10.1038/nature11921](https://doi.org/10.1038/nature11921); pmid: 23407494
39. F. Rohwer *et al.*, The complete genomic sequence of the marine phage Roseophage SIO1 shares homology with nonmarine phages. *Limnol. Oceanogr.* **45**, 408–418 (2000). doi: [10.4319/lo.2000.45.2.0408](https://doi.org/10.4319/lo.2000.45.2.0408)
40. S. Roux *et al.*, Ecology and evolution of viruses infecting uncultivated SUP05 bacteria as revealed by single-cell- and meta-genomics. *eLife* **3**, e03125 (2014). doi: [10.7554/eLife.03125](https://doi.org/10.7554/eLife.03125); pmid: 25171894
41. C. M. Mizuno, F. Rodriguez-Valera, N. E. Kimes, R. Ghai, Expanding the marine virosphere using metagenomics. *PLoS Genet.* **9**, e1003987 (2013). doi: [10.1371/journal.pgen.1003987](https://doi.org/10.1371/journal.pgen.1003987); pmid: 24348267
42. B. L. Hurwitz, A. H. Westveld, J. R. Brum, M. B. Sullivan, Modeling ecological drivers in marine viral communities using comparative metagenomics and network analyses. *Proc. Natl. Acad. Sci. U.S.A.* **111**, 10714–10719 (2014). doi: [10.1073/pnas.1319778111](https://doi.org/10.1073/pnas.1319778111); pmid: 25002514
43. P. Kukkaro, D. H. Bamford, Virus-host interactions in environments with a wide range of ionic strengths. *Environ. Microbiol. Rep.* **1**, 71–77 (2009). doi: [10.1111/j.1758-2229.2008.00007.x](https://doi.org/10.1111/j.1758-2229.2008.00007.x); pmid: 23765723
44. K. E. Wommack, R. R. Colwell, Virioplankton: Viruses in aquatic ecosystems. *Microbiol. Mol. Biol. Rev.* **64**, 69–114 (2000). doi: [10.1128/MMBR.64.1.69-114.2000](https://doi.org/10.1128/MMBR.64.1.69-114.2000); pmid: 10704475
45. V. Dang, M. B. Sullivan, Emerging methods to study bacteriophage infection at the single-cell level. *Front. Microbiol.* **5**, 724 (2014).
46. L. D. Talley, G. L. Pickard, W. J. Emery, J. H. Swift, *Descriptive Physical Oceanography: An Introduction* (Elsevier, Boston, ed. 6, 2011).
47. D. B. Olson, R. H. Evans, Rings of the Agulhas current. *Deep Sea Res. Pt. I* **33**, 27–42 (1986). doi: [10.1016/0198-0149\(86\)90106-8](https://doi.org/10.1016/0198-0149(86)90106-8)
48. E. Villar, Dispersal and remodeling of plankton communities by Agulhas rings. *Science* **348**, 1261447 (2015).
49. M. Breitbart, F. Rohwer, Here a virus, there a virus, everywhere the same virus? *Trends Microbiol.* **13**, 278–284 (2005). doi: [10.1016/j.tim.2005.04.003](https://doi.org/10.1016/j.tim.2005.04.003); pmid: 15936660
50. G. Lima-Mendez *et al.*, Top-down determinants of ocean microbial community structure. *Science* **348**, 1262073 (2015).
51. D. M. Needham *et al.*, Short-term observations of marine bacterial and viral communities: Patterns, connections and resilience. *ISME J.* **7**, 1274–1285 (2013). doi: [10.1038/ismej.2013.19](https://doi.org/10.1038/ismej.2013.19); pmid: 23446831
52. C.-E. T. Chow, D. Y. Kim, R. Sachdeva, D. A. Caron, J. A. Fuhrman, Top-down controls on bacterial community structure: Microbial network analysis of bacteria, T4-like viruses and protists. *ISME J.* **8**, 816–829 (2014). doi: [10.1038/ismej.2013.199](https://doi.org/10.1038/ismej.2013.199); pmid: 24196323
53. A. Longhurst, *Ecological Geography of the Sea* (Elsevier, London, 2007).
54. S. Pesant *et al.*, Open science resources for the discovery and analysis of Tara Oceans data. (<http://biorxiv.org/content/early/2015/05/08/019117>)
55. A. Aminot, R. Kerouel, S. C. Coverly, in *Practical Guidelines for the Analysis of Seawater*, O. Wurl, Eds. (CRC Press, Boca Raton, FL, 2009), pp. 143–178.
56. J. Ras, H. Claustre, J. Uitz, Spatial variability of phytoplankton pigment distributions in the Subtropical South Pacific Ocean: Comparison between *in situ* and predicted data. *Biogeosciences* **5**, 353–369 (2008). doi: [10.5194/bg-5-353-2008](https://doi.org/10.5194/bg-5-353-2008)
57. L. Van Heukelem, C. S. Thomas, Computer-assisted high-performance liquid chromatography method development with applications to the isolation and analysis of phytoplankton pigments. *J. Chromatogr. A* **910**, 31–49 (2001). doi: [10.1016/S0378-4347\(00\)00603-4](https://doi.org/10.1016/S0378-4347(00)00603-4); pmid: 11263574
58. J. M. Gasol, P. A. del Giorgio, Using flow cytometry for counting natural planktonic bacteria and understanding the structure of planktonic bacterial communities. *Sci. Mar.* **64**, 197–224 (2000).
59. M. D. Abramoff, P. J. Magalhaes, S. J. Ram, Image processing with ImageJ. *Biophot. Int.* **11**, 36–42 (2004).
60. S. Schloissnig *et al.*, Genomic variation landscape of the human gut microbiome. *Nature* **493**, 45–50 (2013). doi: [10.1038/nature11711](https://doi.org/10.1038/nature11711); pmid: 23222524
61. R. Luo *et al.*, SOAPdenovo2: An empirically improved memory-efficient short-read de novo assembler. *GigaScience* **1**, 18 (2012). doi: [10.1186/2047-217X-1-18](https://doi.org/10.1186/2047-217X-1-18); pmid: 23587118
62. J. R. Kultima *et al.*, MOCAT: A metagenomics assembly and gene prediction toolkit. *PLoS ONE* **7**, e47656 (2012). doi: [10.1371/journal.pone.0047656](https://doi.org/10.1371/journal.pone.0047656); pmid: 23082188
63. D. Hyatt *et al.*, Prodigal: Prokaryotic gene recognition and translation initiation site identification. *BMC Bioinformatics* **11**, 119 (2010). doi: [10.1186/1471-2105-11-119](https://doi.org/10.1186/1471-2105-11-119); pmid: 20211023
64. S. Roux, M. Krupovic, D. Debroas, P. Forterre, F. Enault, Assessment of viral community functional potential from viral metagenomes may be hampered by contamination with cellular sequences. *Open Biol.* **3**, 130160 (2013). doi: [10.1098/rsob.130160](https://doi.org/10.1098/rsob.130160); pmid: 24335607
65. R. D. Finn, J. Clements, S. R. Eddy, HMMER web server: Interactive sequence similarity searching. *Nucleic Acids Res.* **39** (suppl), W29–W37 (2011). doi: [10.1093/nar/gkr367](https://doi.org/10.1093/nar/gkr367); pmid: 21593126
66. B. Langmead, S. L. Salzberg, Fast gapped-read alignment with Bowtie 2. *Nat. Methods* **9**, 357–359 (2012). doi: [10.1038/nmeth.1923](https://doi.org/10.1038/nmeth.1923); pmid: 22388286
67. J. Oksanen *et al.*, vegan: Community Ecology Package, R package version 2.1-27/r2451 (R Core Team, Vienna, 2013).
68. R Core Team, *R: A Language and Environment for Statistical Computing*, version 2.15.2 (R Core Team, Vienna, 2012).
69. S. N. Wood, Fast stable restricted maximum and marginal likelihood estimation of semiparametric generalized linear models. *J. R. Stat. Soc. Series B Stat. Methodol.* **73**, 3–36 (2011). doi: [10.1111/j.1467-9868.2010.00749.x](https://doi.org/10.1111/j.1467-9868.2010.00749.x)

ACKNOWLEDGMENTS

We thank J. Czekanski-Moir for advice on statistics and L. Coppola for assistance with validating nutrient data. We thank the commitment of the following people and sponsors: CNRS (in particular Groupement de Recherche GDR3280), European Molecular Biology Laboratory (EMBL), Genoscope/CEA, VIB KU Leuven, Stazione Zoologica Anton Dohrn, University of Milano-Bicocca, Fund for Scientific Research—Flanders, Rega Institute, KU Leuven, The French Ministry of Research, the French Government “Investissements d’Avenir” programmes OCEANOMICS (ANR-11-BTBR-0008), FRANCE GENOMIQUE (ANR-10-INBS-09-08), MEMO LIFE (ANR-10-LABX-54), Paris Sciences et Lettres (PSL) Research University (ANR-11-IDEX-0001-02), ANR (projects POSEIDON/ANR-09-BLAN-0348, PHYTBAC/ANR-2010-1709-01, PROMETHEUS/ANR-09-PCS-GENM-217, TARA-GIRUS/ANR-09-PCS-GENM-218), European Union 7th Framework Programme (MicroB3/No.287589, IHMS/HEALTH-F4-2010-261376), European Research Council (ERC) advanced grant award to C.B. (Diatomite: 294823), Gordon and Betty Moore Foundation grant (3790) to M.B.S., Spanish Ministry of Science and Innovation grant CGL2011-26848/BOS MicroOcean PANGENOMICS to S.G.A., TANIT (CONES 2010-0036) from the Agencia de Gestió d’Ajusts Universitaris i Reserca to S.G.A., Japan Society for the Promotion of Science KAKENHI grant 26430184 to H.O., The Research Foundation—Flanders (FWO), BIO5, Biosphere 2 to M.B.S., and the Gordon and Betty Moore Foundation through grants GBMF2631 and GBMF3790 to M.B.S. We also thank the support and commitment of Agnès B. and Etienne Bourgois, the Veolia Environment Foundation, Région Bretagne, Lorient Agglomération, World Courier, Illumina, the Education for Development Foundation, Foundation for Biodiversity Research (FRB), the Prince Albert II de Monaco Foundation, the Tara schooner and its captains and crew. We thank MERCATOR-CORIOLIS and ACRI-ST for providing daily satellite data during the expedition. We are also grateful to the French Ministry of Foreign Affairs for supporting the expedition and to the countries who graciously granted sampling permissions. Tara Oceans would not exist without continuous support from 23 institutes (<http://oceans.taraexpeditions.org>). We also acknowledge excellent assistance from the European Bioinformatics Institute (EBI), in particular G. Cochrane and P. ten Hoopen, as well as the EMBL Advanced Light Microscopy Facility (ALMF), in particular R. Pepperkok. The authors further declare that all data reported herein are fully and freely available from the date of publication, with no restrictions, and that all of the samples, analyses, publications, and ownership of data are free from legal entanglement or restriction of any sort by the various nations whose waters the Tara Oceans expedition sampled in. Data described herein is available at EBI (project identifiers PRJEB402 and PRJEB7988) and PANGAEA (see table S1), and the data release policy regarding future public release of Tara Oceans data is described in Pesant *et al.* (54). We also acknowledge support from University of Arizona (UA) High Performance Computing and High Throughput Computing; the foundation for France-American Cultural Exchange, Partner University Fund program, awarded to Ecole Normale Supérieure and UA; and a grant to UA Ecosystem Genomics Institute through the UA Technology and Research Initiative Fund

and the Water, Environmental, and Energy Solutions Initiative. All authors approved the final manuscript. This article is contribution number 23 of the *Tara* Oceans Expedition. Supplement contains additional data.

Tara Oceans Coordinators

Silvia G. Acinas,¹ Peer Bork,^{2,3} Emmanuel Boss,⁴ Chris Bowler,⁵ Colomán de Vargas,^{6,7} Michael Follows,⁸ Gabriel Gorsky,^{9,31} Nigel Grimsley,^{10,11} Pascal Hingamp,¹² Daniele Iudicone,¹³ Olivier Jaillon,^{14,15,16} Stefanie Kandels-Lewis,^{2,17} Lee Karp-Boss,¹⁸ Eric Karsenti,^{5,17} Uros Krzic,¹⁹ Fabrice Not,^{6,7} Hiroyuki Ogata,²⁰ Stéphane Pesant,^{21,22} Jeroen Raes,^{23,24,25} Emmanuel G. Reynaud,²⁶ Christian Sardet,^{27,28} Mike Sieracki,²⁹ Sabrina Speich,³⁰ ‡ Lars Stemmann,^{9,31} Matthew B. Sullivan,³² Shinichi Sunagawa,² Didier Velayoudon,³³ Jean Weissenbach,^{14,15,16} Patrick Wincker^{14,15,16}

¹Department of Marine Biology and Oceanography, Institute of Marine Sciences (ICM)-CSIC, Pg. Marítim de la Barceloneta 37-49, E08003 Barcelona, Spain. ²Structural and Computational Biology, European Molecular Biology Laboratory, Meyerhofstrasse 1, 69117 Heidelberg, Germany. ³Max-Delbrück-Centre for Molecular Medicine, 13092 Berlin, Germany. ⁴School of Marine Sciences, University of Maine, Orono, ME 04469, USA. ⁵Institut de Biologie de l' Ecole Normale Supérieure (IBENS), and INSERM U1024, and CNRS UMR 8197, 75005 Paris, France. ⁶CNRS, UMR 7144, Station Biologique de Roscoff, Place Georges Teissier, 29680 Roscoff, France. ⁷Sorbonne Universités, Université Pierre et Marie Curie, Univ Paris 06, and UMR 7144, Station Biologique de Roscoff, Place Georges Teissier, 29680 Roscoff, France. ⁸Department of Earth, Atmospheric, and Planetary Sciences,

Massachusetts Institute of Technology, Cambridge, MA 02139, USA. ⁹CNRS, UMR 7093, Laboratoire d'océanographie de Villefranche (LOV), Observatoire Océanologique, 06230 Villefranche-sur-mer, France. ¹⁰CNRS UMR 7232, Biologie Intégrative des Organismes Marins (BIOM), Avenue du Fontaulé, 66650 Banyuls-sur-Mer, France. ¹¹Observatoire Océanologique de Banyuls (OOB), Sorbonne Universités, Pierre et Marie Curie Paris 06, Avenue du Fontaulé, 66650 Banyuls-sur-Mer, France. ¹²Aix Marseille Université, CNRS IGS UMR 7256 13288 Marseille, France. ¹³Stazione Zoologica Anton Dohrn, Villa Comunale, 80121 Naples, Italy. ¹⁴Genoscope, Commissariat à l'Energie Atomique (CEA)—Institut de Génétique, 2 rue Gaston Crémieux, 91057 Evry, France. ¹⁵CNRS, UMR 8030, CP5706, 91057 Evry, France. ¹⁶Université d'Evry, UMR 8030, CP5706, 91057 Evry, France. ¹⁷Directors' Research, European Molecular Biology Laboratory Meyerhofstrasse 1 69117 Heidelberg, Germany. ¹⁸School of Marine Sciences, University of Maine, Orono, ME 04469, USA. ¹⁹Cell Biology and Biophysics, European Molecular Biology Laboratory, Meyerhofstrasse 1, 69117 Heidelberg, Germany. ²⁰Institute for Chemical Research, Kyoto University, Gokasho, Uji, Kyoto 611-0001, Japan. ²¹PANGAEA, Data Publisher for Earth and Environmental Science, University of Bremen, 28359 Bremen, Germany. ²²MARUM, Center for Marine Environmental Sciences, University of Bremen, 28359 Bremen, Germany. ²³Department of Microbiology and Immunology, Rega Institute, KU Leuven, Herestraat 49, 3000 Leuven, Belgium. ²⁴Center for the Biology of Disease, VIB KU Leuven, Herestraat 49, 3000 Leuven, Belgium. ²⁵Department of Applied Biological Sciences, Vrije Universiteit Brussel, Pleinlaan 2, 1050 Brussels, Belgium. ²⁶The Rlab, University College Dublin, Belfield, Dublin, Ireland. ²⁷Biodev, Observatoire Océanologique, CNRS, UMR

7009, 06230 Villefranche-sur-mer, France. ²⁸Sorbonne Universités, Université Pierre et Marie Curie, Univ Paris 06, UMR 7009 Biodev, 06230 Observatoire Océanologique, Villefranche-sur-mer, France. ²⁹Bigelow Laboratory for Ocean Science, East Boothbay, ME 04544, USA. ³⁰Laboratoire de Physique des Océans, Institut Universitaire Européen de la Mer, Université de Bretagne Occidentale (UBO-IUEM), Place Copernic, 29820 Plouzané, France. ³¹Sorbonne Universités, Université Pierre et Marie Curie, Univ Paris 06, UMR 7093, Laboratoire d'océanographie de Villefranche (LOV), Observatoire Océanologique, 06230, Villefranche-sur-mer, France. ³²Department of Ecology and Evolutionary Biology, Depts Molecular and Cellular Biology and Soil, Water and Environmental Science, University of Arizona, Tucson, AZ 85721, USA. ³³DVIP Consulting, 92310 Sèvres, France. †Present address: National Science Foundation, Arlington, VA 22230, USA. ‡Present address: Department of Geosciences, Laboratoire de Météorologie Dynamique (LMD), Ecole Normale Supérieure, 24 rue L'homond 75231 Paris, Cedex 05, France. §Present address: Department of Microbiology, Ohio State University, Columbus, OH 43210, USA.

SUPPLEMENTARY MATERIALS

www.sciencemag.org/content/348/6237/1261498/suppl/DC1
File S1

References
Databases

19 September 2014; accepted 25 February 2015
10.1126/science.1261498

This copy is for your personal, non-commercial use only.

If you wish to distribute this article to others, you can order high-quality copies for your colleagues, clients, or customers by [clicking here](#).

Permission to republish or repurpose articles or portions of articles can be obtained by following the guidelines [here](#).

The following resources related to this article are available online at www.sciencemag.org (this information is current as of May 21, 2015):

Updated information and services, including high-resolution figures, can be found in the online version of this article at:

<http://www.sciencemag.org/content/348/6237/1261498.full.html>

Supporting Online Material can be found at:

<http://www.sciencemag.org/content/suppl/2015/05/20/348.6237.1261498.DC1.html>

A list of selected additional articles on the Science Web sites **related to this article** can be found at:

<http://www.sciencemag.org/content/348/6237/1261498.full.html#related>

This article **cites 62 articles**, 18 of which can be accessed free:

<http://www.sciencemag.org/content/348/6237/1261498.full.html#ref-list-1>

This article has been **cited by** 3 articles hosted by HighWire Press; see:

<http://www.sciencemag.org/content/348/6237/1261498.full.html#related-urls>

This article appears in the following **subject collections**:

Geochemistry, Geophysics

http://www.sciencemag.org/cgi/collection/geochem_phys

Microbiology

<http://www.sciencemag.org/cgi/collection/microbio>